Cryogenic (70K) Measurement of an All-Composite 2-Meter Diameter Mirror

Brian Catanzaro [a*], Steven Connell [b], Mark Mimovich [b], Stan Backovsky [b], Grant Williams [b], James A.Thomas [c], Dan Barber [c], Roger Johnston [c], Joe Hylton [b], Kelly Dodson [b], and Eri Cohen [d]

[a]CFE Services, 5147 Pacifica Dr, San Diego, CA 92109
[b]Composite Optics Incorporated, 9617 Distribution Ave, San Diego, CA 92121
[c]Light Works Optics, Inc., 2691 Richter Ave., Suite 105, Irvine CA 92606
[d] Jet Propulsion Laboratory, California Institute of Technology,
4800 Oak Grove Drive, Pasadena CA 91109

ABSTRACT

The Herschel Space Observatory (formerly known as FIRST) consists of a 3.5 m space telescope. As part of a JPL-funded effort to develop lightweight telescope technology suitable for this mission, COI designed and fabricated a spherical, F/1, 2 m aperture prototype primary mirror using solely carbon fiber reinforced polymer (CFRP) materials. To assess the performance of this technology, optical metrology of the mirror surface was performed from ambient to an intended operational temperature for IR-telescopes of 70K. Testing was performed horizontally in a cryogenic vacuum chamber at Arnold Engineering Development Center (AEDC), Tennessee. The test incorporated a custom thermal shroud, a characterization and monitoring of the dynamic environment, and a stress free mirror mount. An IR-wavelength phase shifting interferometer (IR PSI) was the primary instrument used to measure the mirror surface. From an initial surface figure of 2.1 microns RMS at ambient, a modest 3.9 microns of additional RMS surface error was induced at 70K. The thermally induced error was dominated by low-order deformations, of the type that could easily be corrected with secondary or tertiary optics. In addition to exceptional thermal stability, the mirror exhibited no significant change in the figure upon returning to room temperature.

Keywords: Lightweight Mirrors, Cryogenic Testing, Composite Materials, Phase Shifting Interferometer, Thermal Shroud, Vacuum Test Chamber, Vibration Measurements, Quilting, High Spatial Frequency Errors

1. INTRODUCTION

The Herschel Space Observatory (formerly known as FIRST), is a European Space Agency (ESA) cornerstone mission, that will be used for photometry, imaging and spectroscopy in the 80 to 670 μm range (see Figure 1). The key science goals that this observatory will achieve concern how galaxies formed in the early universe, and how stars form, and have been forming, throughout the history of the universe. NASA, through the Jet Propulsion Laboratory (JPL), has contributed to the telescope and its design. [1] This paper will discuss the work done by JPL, Composite Optics, Incorporated (COI), and Light Works Optics, Incorporated (LWO) to characterize a large aperture (2 m) demonstration mirror at 70 K. Requirements traceable to the Herschel Space Observatory are wavefront error (6 μm RMS), mass (280 kg), primary mirror diameter (3.5 m), F-number (F/0.5), and the operational temperature (70 – 90 K).

* Correspondence: bcatanza@alumni.caltech.edu Tel: (858) 204-6299

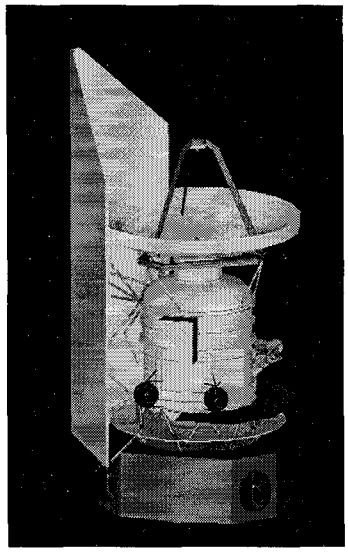

Figure 1: Herschel Space Observatory

In response to the telescope requirements a low mass, low coefficient of thermal expansion (CTE) telescope [1] has been designed using carbon fiber reinforced polymer (CFRP) and a 2 m diameter demonstration mirror was fabricated [2] for the purpose of cryogenic performance characterization (see Figure 2). The 2 m diameter demonstration mirror is spherical in shape with a radius of curvature of 4.2 m. It is coated with a protected gold and has an areal density of 10.1 kg/m^2. The mirror has a unique, segmented facesheet. The core that supports the facesheet is contiguous, but the facesheet is separated into six (6) petals. A specific goal for the demonstration mirror was the optical characterization of surface errors at 70 K.

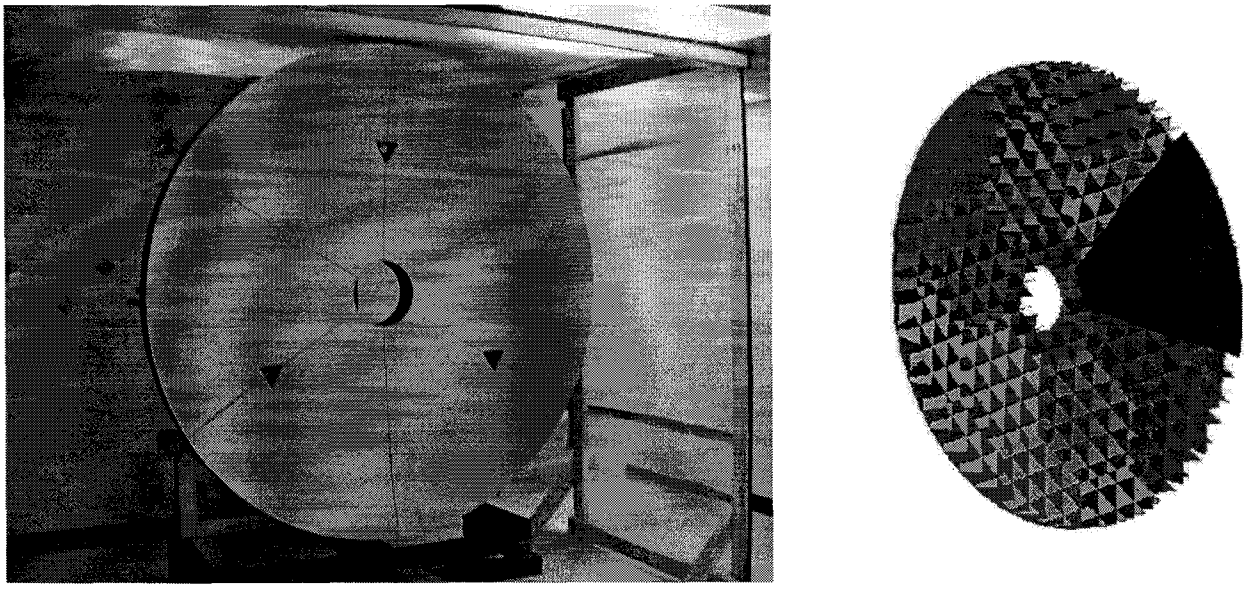

Figure 2: 2 m CRFP Lightweight Demonstration Mirror (10.1 kg/m^2)

Several features of the carbon fiber 2 m mirror differentiate it from traditional mirrors. [2] The material, carbon fiber reinforce polymer (CFRP), is an extremely low expansion material even at cryogenic temperatures. The manufacturing process involved curing the facesheets on a mold in order to generate a smooth near net shape surface and an assembly technique that created the final figure of the mirror. Although the manufacturing mold was polished, the mirror itself was never polished. The stiffness of the mirror met all of the launch requirements traceable to the Herschel Space Observatory. However, it was sufficiently lightweighted that gravity did affect the surface figure. Generally the surface figure was

specular (surface roughness: 0.6 μm RMS from profilometry data). Material uniformity was closely controlled and bond lines were minimized to ensure minimal quilting upon exposure to cryogenic temperatures. However, some quilting was anticipated.

Several methods exist for the characterization of the 2 m demonstration mirror. After a survey of methods and preliminary testing, an infrared phase shifting interferometer (IR PSI) and an infrared Shack-Hartmann (IR SH) wavefront sensor were chosen to collect cryogenic characterization data. [3] Due to the nature of the 2 m demonstration mirror's construction, the cryogenic test data from the IR SH were not satisfactory. As such, only the data from the IR PSI are reported here.

The Herschel Space Observatory required surface error data with a high density of data points across the entire aperture. Specific requirements on low-order aberrations, quilting, and stray light mandated more than 100 data points across the diameter.

The goals for the characterization were to:

1. Determine the deformation in the mirror as a result of exposure to cryogenic temperature (70 K),
2. Identify any change in figure after cycling the mirror to cryogenic temperature,
3. Separate figure changes into low order errors (potentially correctable with the secondary mirror) and high order terms (uncorrectable due to the telescope's field of view),
4. Characterize high spatial frequency figure changes (i.e. quilting, gap effects, and mirror interface distortions),
5. Collect data necessary for further optimization of the mirror design.

All of the goals for the characterization were met. To provide a context for the measurement, a review of the experiences gained during a previous cryogenic test (October 1999) of the mirror is presented. The test configuration for the most recent characterization (May 2000) is discussed including a description of the facilities, the efforts to manage the thermal environment of the test mirror, and a survey of the dynamic environment of the test area. The optical metrology instruments are described and the test results are summarized. In addition, the test results are interpreted in the context of a composite telescope design for the Herschel Space Observatory.

2. REVIEW OF PRIOR TEST DATA

The 2 m demonstration mirror was previously tested (October 1999) at cryogenic temperatures. [2] This characterization was limited to 200 K and did not result in data sufficient to support the design of a composite telescope for the Herschel Space Observatory. Although the information was incomplete, it provided valuable insight into four areas that were subsequently addressed prior to the most recent test. These areas were (in order of importance): instrument limitations, thermal management, data reduction techniques, and interferogram signal strength.

The most important information gained during the October 1999 test was the limitations of the existing interferometer. The infrared (λ = 10.6 μm) interferometer used for the characterization was designed and manufactured by Breault Research Organization, Incorporated (BRO) in the mid to late 1980's. The resolution and dynamic range of this instrument were insufficient for full characterization of the 2 m demonstration mirror at 70 K. As a consequence, prior to retesting in May 2000, the interferometer was upgraded by replacing the pyroelectric vidicon detector with a state of the art microbolometer array, fabricating a custom F/2 objective, and correcting the aberrations in the pupil relay imaging optics. [3]

Another valuable insight gained from the earlier test was the rate of cooling for the mirror. The primary mechanism for cooling was radiant heat transfer. Predictions of the rate of cooling for the mirror indicated a lengthy and costly cycle time to achieve the target temperature of 70 K with minimal thermal gradients. As a consequence, efforts were taken to design a thermal shroud to enhance the cooling rate. The shroud was also designed to improve the gradient across the face of the mirror from 22 K (test data from October 1999) to less than 5 K and the gradient from front to back from 6 K (test data from October 1999) to less than 5 K.

The processing of the interferograms can be highly dependent on the algorithms used for phase unwrapping. Low contrast fringes and high fringe densities can cause unsophisticated algorithms to produce phase discontinuities. These discontinuities can be identified fairly easily but they are difficult to remove. More advanced phase unwrapping algorithms became available in the Intelliwave™ interferometer software from Engineering Synthesis Design. These algorithms were instrumental in reducing the data collected into surface error maps.

Given the challenges of the test it was decided to increase the signal returning to the interferometer by applying a reflective gold coat to the mirror. The initial test was conducted using an uncoated mirror (Fresnel reflection). The low return from the mirror made the processing of the data challenging. The increase in return signal improved both the brightness and contrast of the fringes. It was speculated that the application of the coating would change the figure of the 2 m demonstration mirror. Testing demonstrated that these changes could not be measured and were deemed inconsequential compared to the benefits.

3. TEST FACILITY

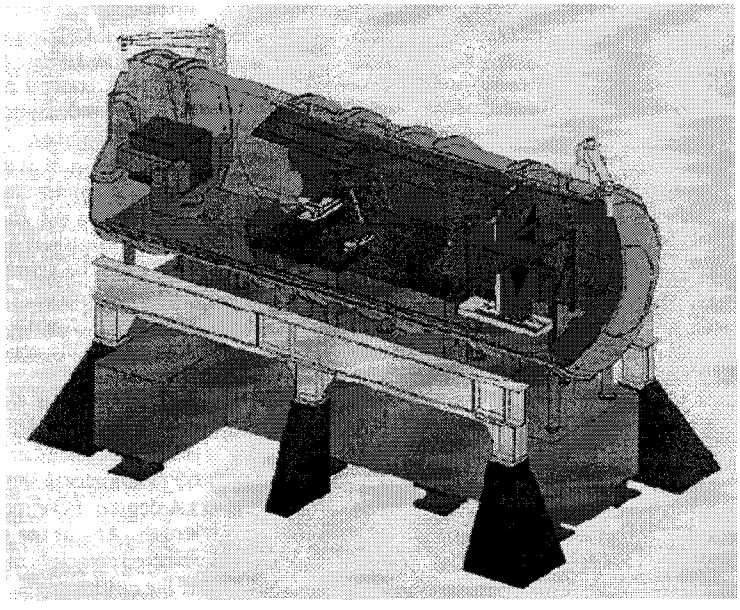

Figure 3: AEDC Mark 10V Chamber

The facility selected for the optical testing was the Mark 10V chamber (see Figure 3) at the Arnold Engineering Development Center (AEDC). AEDC is operated by the United States Air Force Materiel Command Test Center at Arnold Air Force Base, Tennessee. The chamber was located inside a Class 1000 cleanroom. A steel framework attached to a seismic mass supported the test article and the metrology platform. This mass attenuated vibrations from the surrounding disturbance sources. The thermal environment of the chamber was cooled by a shroud that supported both liquid nitrogen and gaseous helium. Lines carrying the liquid nitrogen and gaseous helium were available for custom shrouds internal to the chamber.

The Environmental Test Facility at AEDC consists of an array of thermal-vac chambers capable of reaching hard vacuum (10^{-7} Torr) and 40-50 K at varying rates based on customer specifications. The cooling control systems have the capability of ramping and holding temperature in either direction. The Mark I chamber at AEDC is large enough to test fully deployed satellites and was a candidate facility for hosting the optical tests of the flight telescope for the Herschel Space Observatory.

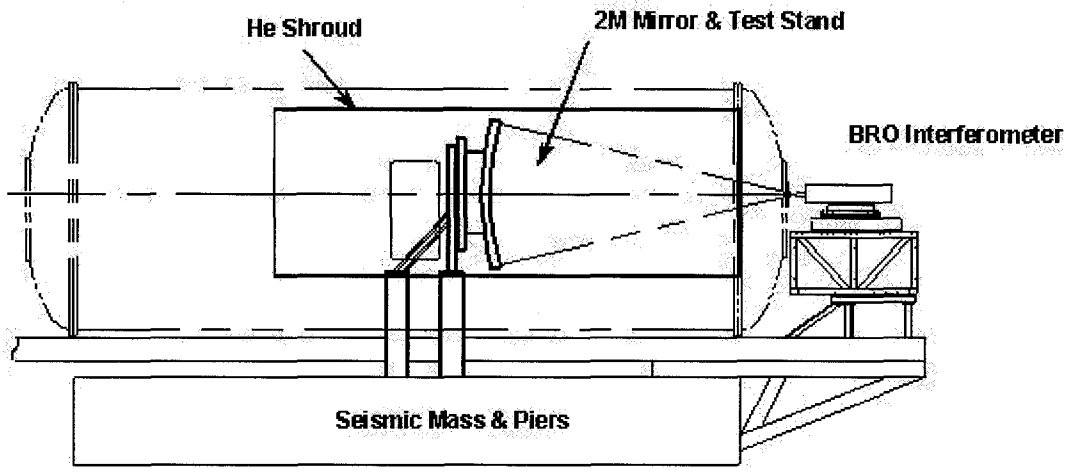

Figure 4: Mirror Test Configuration

The test configuration is diagrammed in Figure 4. The mirror was mounted on a test stand inside of a helium shroud. The test stand was mounted kinematically to pillars connected to the seismic mass. The test stand supported the mirror using a single rod that interfaced to a fitting near the top of the mirror. A small zinc selenide window served as the optical port for the test. The mirror and the chamber were instrumented with thermocouples to monitor the temperature throughout the test. The optical instrumentation was mounted on a metrology platform. This platform consisted of a granite top surface for the instrumentation and a steel framework that connected the platform to the seismic mass.

4. THERMAL MANAGEMENT

Thermal goals of the test were not only to achieve the coldest test temperature, but also to provide opportunities for testing at intermediate temperatures. In addition, the operating environment of the Herschel Space Observatory was specified from 90 K to 70 K. Therefore it was desirable to include a 90 K test temperature. The duration of the test prohibited multiple temperature cycles. However, there was an opportunity to partially heat the mirror to 200 K and then cool it again to 70 K. The final temperature profile for the test is shown in Figure 5. This profile offered opportunities to test the mirror at multiple temperatures as well as investigate the repeatability of the cryogenic surface error.

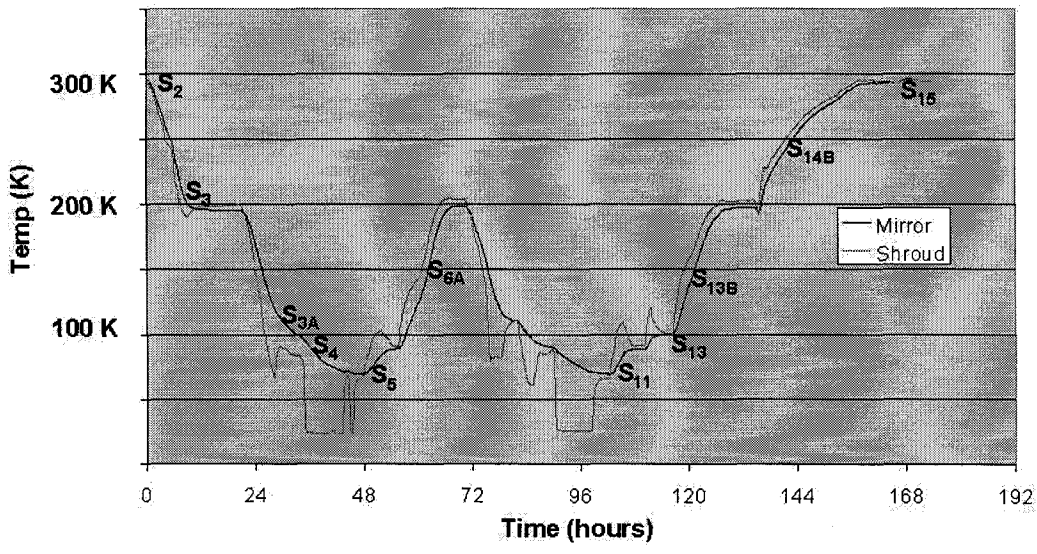

Figure 5: Temperature Profile During Test (S_i Refers to Data Collection Points)

Thermal management in a cryogenic test at 70 K represents a number of challenges. Foremost among these challenges are: thermal gradients and cooling duration. The thermal gradients would affect the accuracy of the test and the cooling duration would affect the cost of the test. The primary heat transfer mechanism for the 2 m demonstration mirror was radiant heat transfer. For that reason, a custom set of shrouds was modeled, designed, and implemented at the test facility.

Two custom shrouds were added to the Mark 10V chamber. One shroud was conically shaped and placed between the front window (optical test port) and the mirror. The second shroud encapsulated the mirror backside, as shown in Figure 6. Both shrouds were cooled using gaseous helium (GHe) lines, which came from the same supply as the Mark 10V sidewall shrouds.

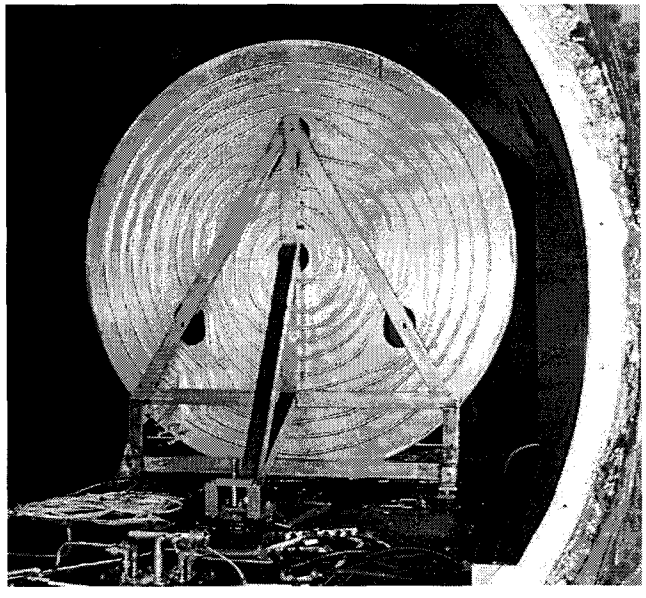

Figure 6: Backside Shroud in chamber

The backside shroud was especially important in isolating the mirror from circumferential gradients seen in the chamber sidewalls at low temperatures. Earlier test data had indicated side-to-side gradients within the sidewall of greater than 50 K. The backside shroud designed for this test was predicted to produce a gradient less than 5 K while operating at a temperature of 70 K. This provided a uniform cold surface by which to cool the 2 m demonstration mirror. As the mirror cooled, the only significant backside gradients were caused by the conductive heat leaks at the mounting locations. This can be seen in the isotherms from the thermal model of the 2 m demonstration mirror (see Figure 7).

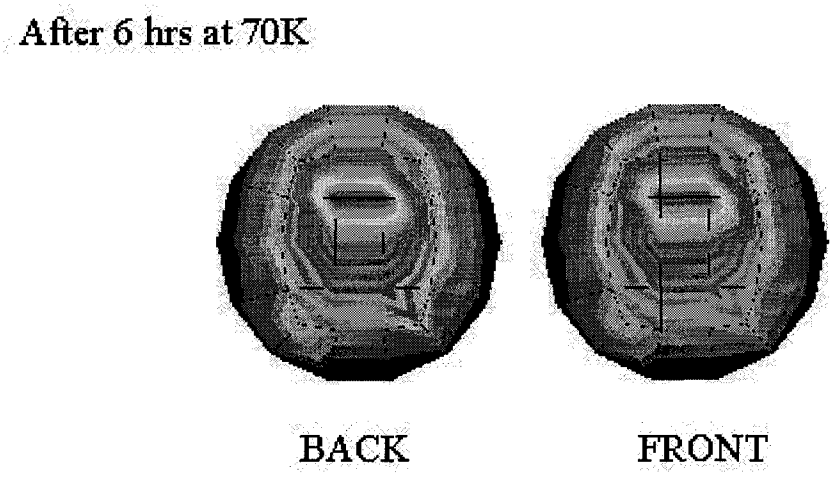

Figure 7: Isotherm from Thermal Model of Mirror (Max Temperature Variation: 1.5K)

Another advantage of the shroud was the dramatic reduction in the time required to cool the mirror. The backshroud had a relatively small thermal mass making it easier to create a uniform temperature background for the mirror. Thus the intermediate temperatures (200 K and at 100 K) required less time to reach steady state. Most importantly, the shroud was predicted to reduce the time to reach 70 K by up to 50% when compared to the standard configuration of the Mark 10V chamber (see Figure 8).

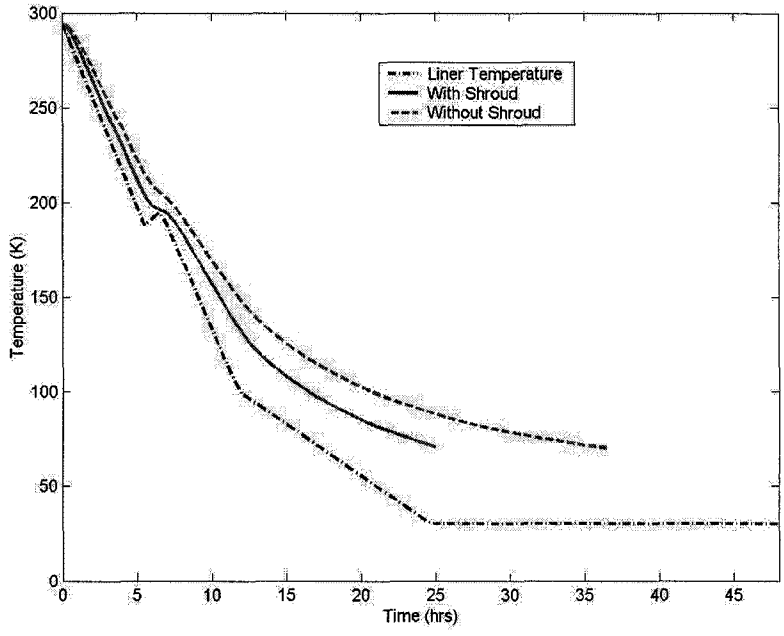

Figure 8: Comparison of Cooling Time With and Without the Shroud

The predicted thermal behavior of the system was compared with the measured temperatures. In order to model the system, cooling times for the shroud had to be assumed. In practice, the actual cooling was faster than the assumed cooling. Therefore, only a loose comparison between the predicted mirror temperature and the actual mirror temperature is possible. However, the response of the mirror to the backshroud was very similar between the predicted and test data (±10 K).

5. VIBRATION ENVIRONMENT

The primary motivation for these measurements was to characterize the dynamics of this facility in order to identify potential disturbances sources and act to either shut them off or employ isolation techniques (rubber pads, Barry-type mounts, etc) to attenuate their influence on the new set of optical measurements. Secondary objectives of these dynamic measurements included:

- Establishment of thresholds for motion of either the mirror or metrology system at which point fringe patterns captured by the CO_2 BRO interferometer become unstable.
- Establish background vibration acceleration, velocity, and displacement levels under various facility operating conditions to serve as a guide for future optical testing.

The magnitude of the velocity and displacements were obtained by integrating the acceleration time-domain signals. Accellerometers, rated for 35 K, collected the time-domain data. This data helped to quantify the amount of motion that existed at the mirror, at the chamber seismic mass piers, at the metrology support frame, and at the interferometer optics. The dynamic data acquisition system was used to collect data at 38 disturbance events using a single setup configuration. There were 7 channels of accelerometer data acquired using the COI data acquisition system and 8 channels of accelerometer data acquired by the AEDC instrumentation group. Of the 38 events acquired using the COI system, 21 were deemed representative and were reduced.

Data was collected at a rate of between 50 – 100 Hz. Synthesized displacement time-domain data were obtained from the acquired acceleration time-history data using MATLAB's explicit 4^{th} and 5^{th} order Runge-Kutta ordinary differential equation solver (ode45). Prior to integrating the acceleration time-history signal, floating ground effects in the measured signal were removed using a linear detrending routine. Once the signal was detrended and scaled, a 5^{th} order Chebyshev type I high-pass filter set at 5 Hz, was used to filter out low frequency bias due to the accelerometer's inaccuracy in the 0 to 3 Hz range. Upon obtaining the synthesized displacement time-domain signal, a peak and RMS value were calculated.

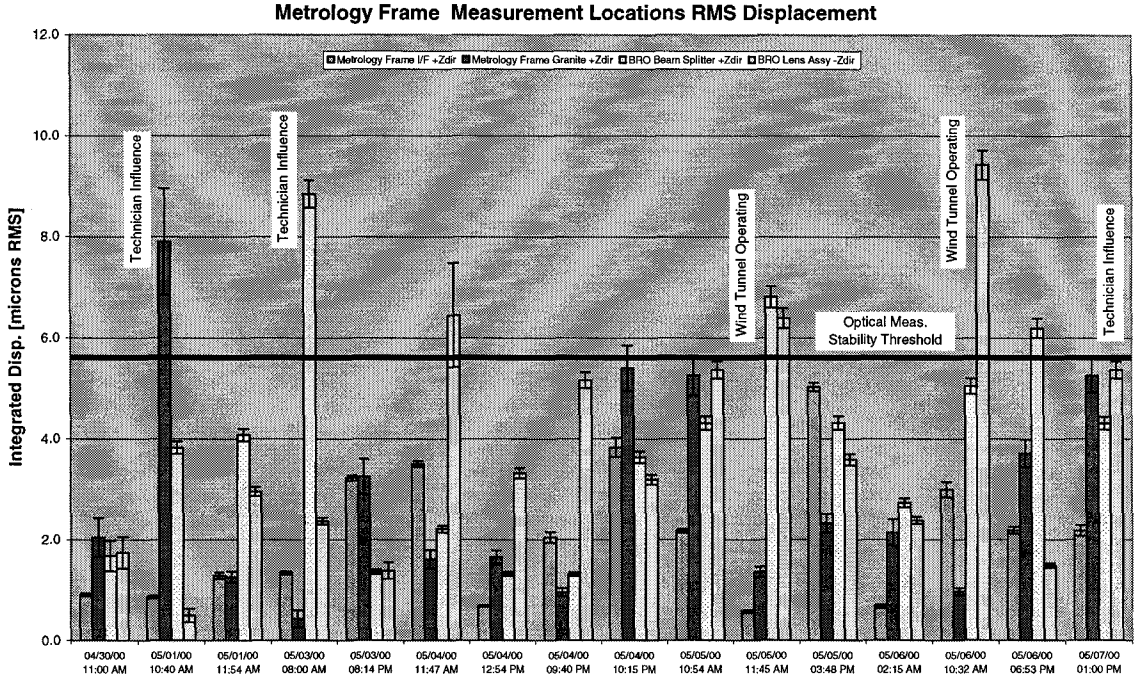

Figure 9: Displacement Histogram – Metrology Frame

In order to graphically illustrate the synthesized displacements obtained from the acceleration measurement events and to determine the optical measurement stability threshold, histograms were constructed for the 21 measurement events processed from the COI data acquisition system and suite of 7 sensors. The histogram for the 4 measurement locations on the Metrology Frame is shown in Figure 9 and the histogram for the 2 measurement locations on the mirror and the 1 location on the chamber pier is shown in Figure 10. Each bar represents one of the synthesized displacements with the calculated uncertainty shown as an error bar. For each of the 21 events, each displacement value is shown, 4 on the Metrology Frame and 3 inside the chamber. In those cases where optical measurements were not possible due to significant instability in the fringe patterns, operating condition notes have been added to these histograms as explanation of the disturbance source(s). As expected, the most disruptive events were human activities (technician involvement), the HVAC system, and the wind tunnel.

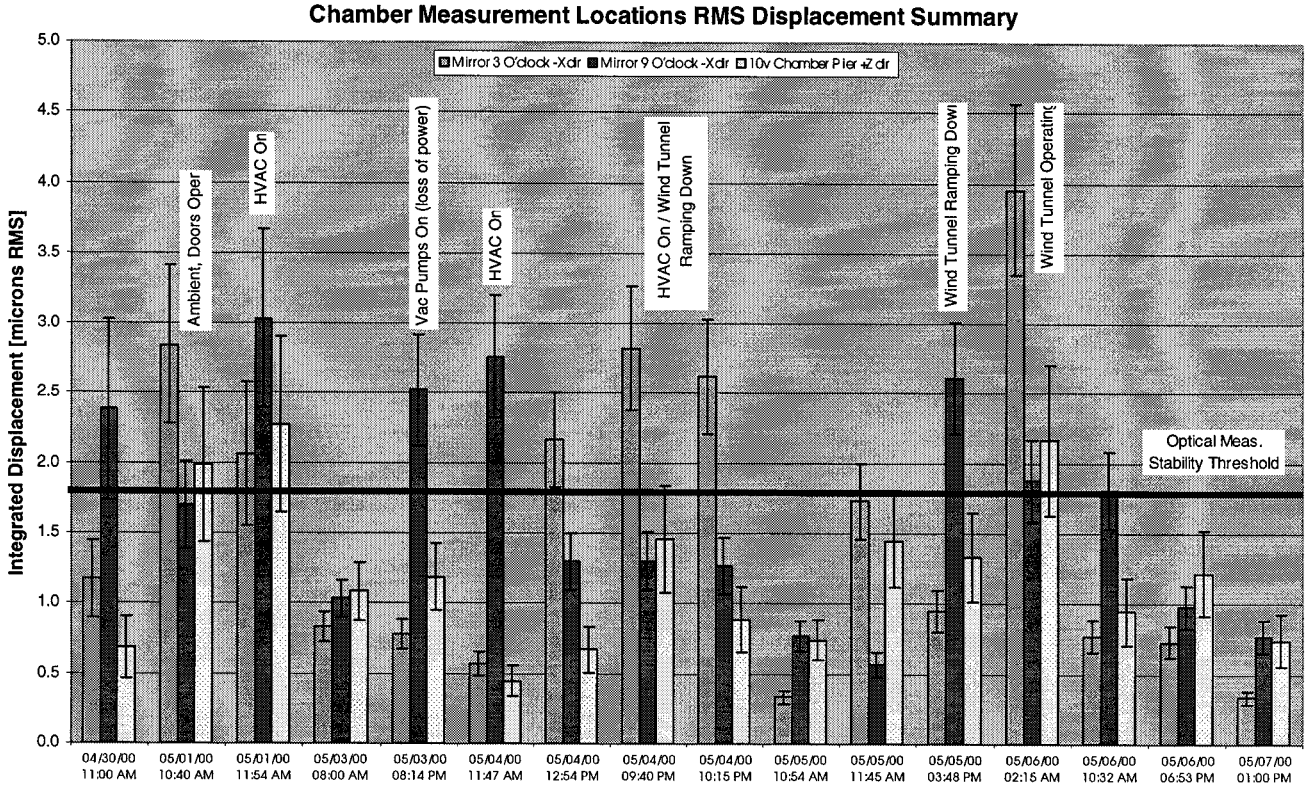

Figure 10: Displacement Histogram – Chamber

Based on the events where optical measurements were and were not possible, an optical measurement stability threshold was established on each histogram. The findings are summarized in Table 1.

Table 1: Experimentally Determined Motion Thresholds.

Optical Component	Motion Threshold
Metrology Frame / Interferometer	5.5 μm (λ/2)
Mirror / Pier	1.8 μm (λ/6)

The conclusions that can be drawn from these measurements are:

- The 10V chamber Seismic mass is very stable and when the near-by wind tunnel is not operating, the sensors used by the AEDC measurement group were not sensitive enough to accurately measure the acceleration levels.
- The seismic motion due to operation of the near-by wind tunnel must have a dominant frequency content which is below the break frequency of the pneumatic isolators used to float the 10V chamber seismic mass, system of support piers, and test article.

6. OPTICAL METROLOGY INSTRUMENTS

The optical test was configured as a center of curvature test, locating the focal point of the objective at the center of curvature of the mirror (see figure 4). Two instruments were aligned with the mirror: the IR PSI and the IR SH. The design of these instruments is detailed in the literature. [3] During the course of measurement, it became clear that the IR SH was not

producing data of the caliber necessary for comparison. Therefore, the IR SH is not described nor are the results from its measurements discussed. The measurements taken with the IR PSI were very successful and provided the data necessary to support the design of the Herschel Space Observatory.

As mentioned previously, the IR PSI manufactured by BRO was modified in order to create an instrument capable of fulfilling the requirements. The instrument used a line narrowed CO_2 source with a coherence length in excess of 10 m. The interferometer was configured as an unequal path system with a piezo driving the phase shifting reference mirror. The pupil was imaged to a room temperature microbolometer camera using a telescope with multiple magnifications (1X, 2X, 4X). The software, Intelliwave™, was used to automate the data collection and reduce the fringe patterns to surface error map data.

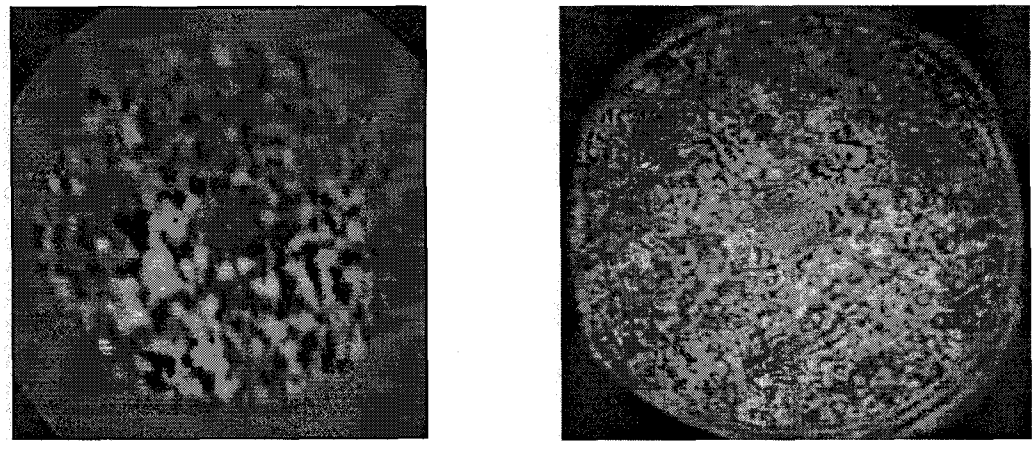

Figure 11: Interferograms of the 2 m Demonstration Mirror Before (Left) and After Modifications (Right) to the IR PSI

The modifications to the IR PSI were to the software, objective lens, sensor, and optics train. Figure 11 shows interferograms of the 2 m demonstration mirror before [2] and after [3] the modifications. After these modifications, the lateral resolution was 16 mm. The slope error cutoff is directly related to the maximum fringe density that limits the lateral resolution. The 60 fringes across the aperture corresponds to 30 waves (10.6 μm) of surface error over 2000 mm. This corresponds to 160 μrad slope error for the 1X magnification, 320 μrad slope error for the 2X magnification, and 640 μrad slope error for the 4X magnification.

7. DATA COLLECTION METHODOLOGY

The goals for the characterization were to:

1. Determine the deformation in the mirror as a result of exposure to cryogenic temperature (70 K),

2. Identify any change in figure after cycling the mirror to cryogenic temperature,

3. Separate figure changes into low order errors (potentially correctable with the secondary mirror) and high order terms (uncorrectable due to the telescope field of view),

6. Characterize high spatial frequency figure changes (i.e. quilting, gap effects, mirror interface distortions).

The data necessary to support these goals included full aperture interferograms recorded at a variety of temperatures (see Figure 5) and high resolution interferograms of the mirror surface to fully characterize the quilting effects.

To collect the full aperture data at each temperature, first the interferometer was aligned to the mirror and nulled (tip, tilt, and focus). A five-bucket algorithm was used for phase shifting. Each surface was the result of calculations based on five (5) interferograms each separated by 90° of phase (0°, 90°, 180°, 270°, 360°). The accuracy of the surface map is very dependent

on the phase angle. Therefore, the piezo movement was calibrated to ensure a 90° phase angle prior to collecting data at any given temperature. Next, a trial interferogram was captured. The results were analyzed for signal strength and fringe contrast. Laser power was adjusted accordingly to maximize signal strength without saturation. Criteria were set for the fringe contrast to automatically reject interferograms that were taken in the presence of excessive vibration. In order to reduce random errors, multiple measurements were taken at each temperature. At each temperature, 30 sets of surface data (five interferograms each) were collected. This process reduced the random error less than $\lambda/50$ (0.2 μm).

Once the data was collected, it was reduced to a single surface map. This process involved first generating a mask to obscure data outside the clear aperture and around the mount points. The mask was defined using fiducials on the mirror and data from a CAD database. This mask was applied to each of the 30 surfaces. The surfaces were then averaged to reduce the noise in any single measurement. After averaging, the full aperture surface map was registered and centered in order to make the differencing process more convenient. The accuracy of the fiducial marks was ± 16 mm.

The high resolution (sub aperture) interferograms were taken during the same measurement cycle as the full aperture data. The sub aperture data were used to understand details about the mirror surface and perform metrology using surface stitching technology. The results of the surface stitching work is presented elsewhere. [4]

Data collection and reduction of the sub aperture measurements was very similar to the full aperture measurements. The key exception was in the nulling process. [4] A reference sphere external to the chamber was used for nulling prior to the collection of data. In this way, each sub aperture shared a common reference point for the intereferometer instead of removing focus, tip, and tilt on each sub aperture.

8. FULL APERTURE TEST RESULTS

The test results are described in three different ways: total surface error, low order surface error, and high order surface error. For the purposes of the analyses in this paper, the surface errors reported are defined as the difference between the initial room temperature measurement and the measurement at temperature. The low order surface error is the surface error after removing all errors higher than the first 36 Zernike terms (University of Arizona convention). The majority of these errors can be removed by figuring the secondary mirror to compensate for the aberrations in the primary mirror. The high order surface error is defined as the residual errors after the first 36 Zernike terms are removed (set to zero).

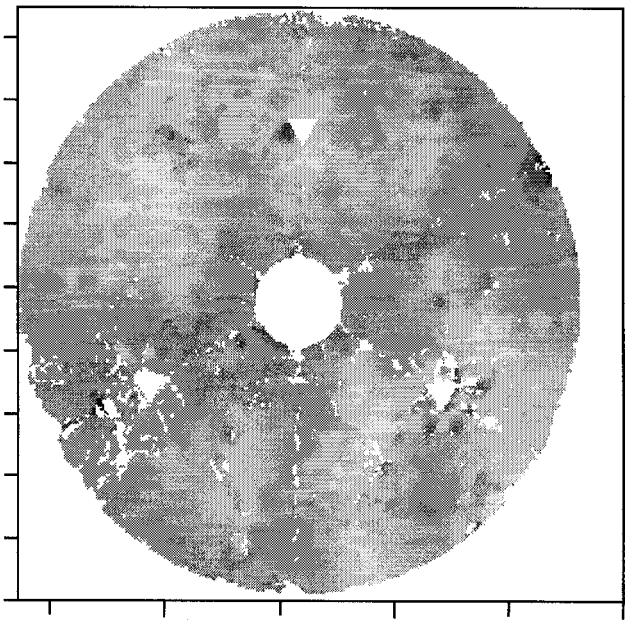

Figure 12: Delta Measurement (293 K to Cryo): 3.9/28 μm PV/RMS

Figure 12 shows the effect of cryogenic temperature (70 K) on the surface of the mirror. The surface error of 3.9 μm RMS demonstrates a highly uniform, relatively stress free fabrication. Recall that the mirror has a unique construction involving a

segmented facesheet with six panels, a segmented backsheet with six panels, and a rib structure continuous across the gaps between the panels, but not continuous across the entire mirror aperture. [2] In fact, the mirror was never polished; each panel was replicated off of a glass mold and assembled using a precision assembly tool. Given this construction, potential surface errors would be generated at the interface between the ribs and the facesheets and at the gaps between the facesheets. There is some evidence of quilting from the rib/facesheet interface but the errors near the gaps between panels are relatively inconsequential.

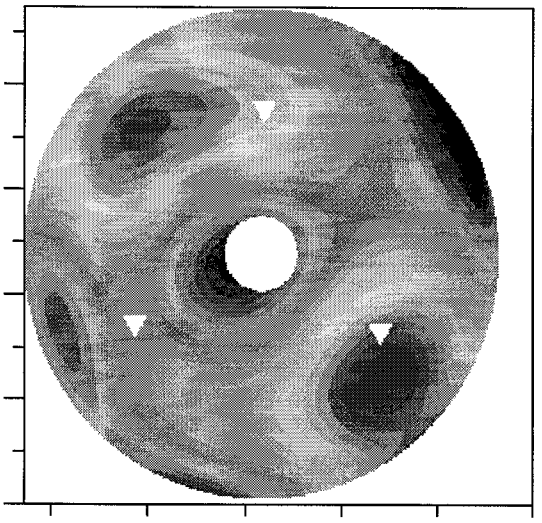

Low Order Figure: 3.4/15 μm PV/RMS

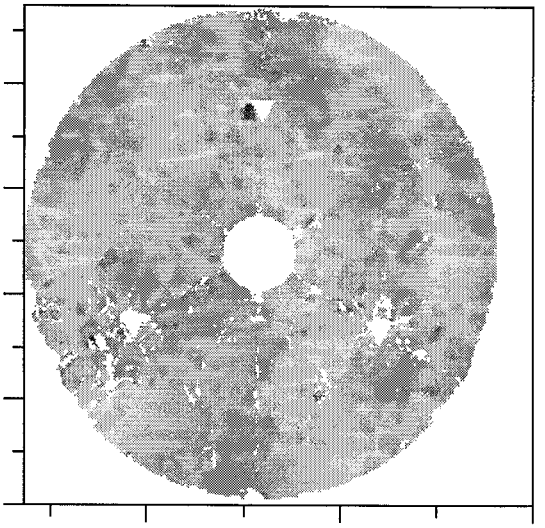

High Order Figure: 1.9/20 μm PV/RMS

Figure 13: Separation of Surface Error into Low and High Order Zernikes

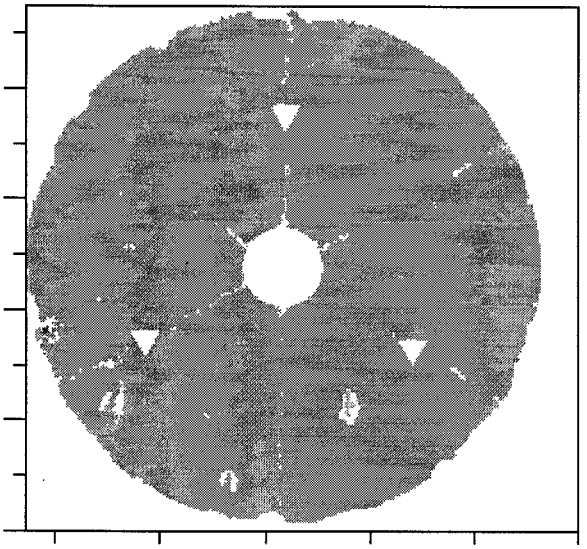

Repeatability Room Temperature: 0.55 μm RMS

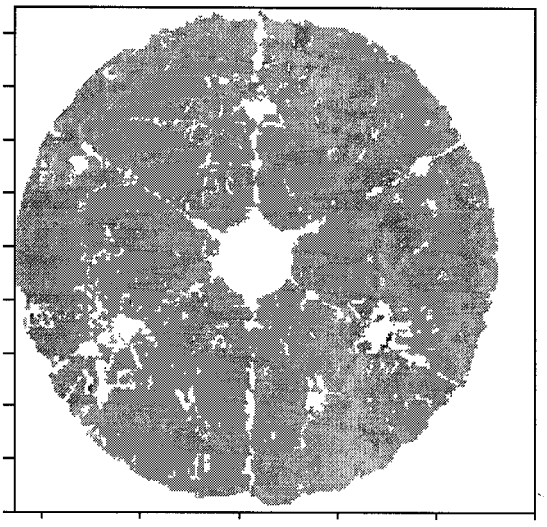

Repeatability 70 K: 0.86 μm RMS

Figure 14: Repeatability of Surface Errors

Figure 13 shows the distribution of errors into low order and high order. The bulk of the errors are low order errors, which can be corrected by figuring the secondary mirror. [5] The high order errors can be described as quilting and hexafoil. The six fold symmetry of hexafoil is undoubted the result of the segmented facesheet/backsheet construction. The hexafoil error has a peak to valley (PV) surface error on the order of 1 μm. Quilting is more prominent than the hexafoil and appears to be generally less than 5 μm peak to valley. Quilting exists across the mirror and will be described further in the sub aperture results.

Figures 14 shows the effect of cycling the mirror. The mirror was exposed to 70 K twice; the second exposure occurred after warming up to 200 K (see Figure 5) and the difference in the surfaces is 0.86 μm RMS. The comparison of room temperature measurements before the start of the test and after the completion of the test resulted in a difference of 0.55 μm RMS.

9. SUB APERTURE TEST RESULTS

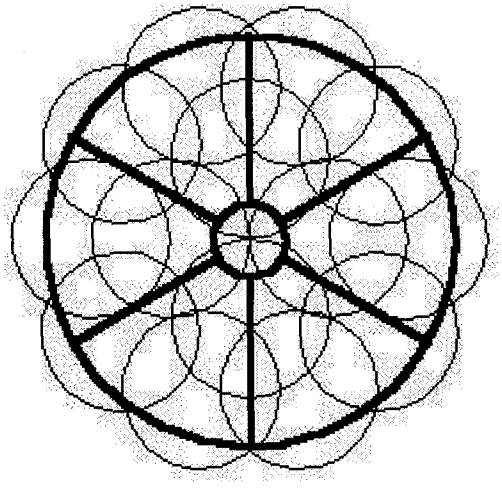

Figure 15: Map of 14 Sub Apertures Where High Resolution Surface Data Was Collected

The high resolution (sub aperture) interferograms were taken to evaluate the quilting effect and observe any surface anomalies. A map of the sub apertures is diagrammed in Figure 15. Severe quilting would appear as a periodic structure identical to the rib pattern supporting the facesheet. A worst case for the Herschel Space Observatory would be a consistent pattern across the mirror producing repeating images in the focal plane like a grating. Other surface anomalies of particular interest were deformations around the fittings and the perimeters of each of the six (6) panels that comprise the facesheet.

After analyzing all of the sub apertures, consistent quilting was not found. Figure 16 shows a series of surface maps that trace a gap between the panels across the diameter of the mirror. Note that along the gap there is little change to the overall surface. Two of the three fittings designed into the mirror appear in Figures 16A, 16C, and 16D. Around these fittings are reinforcements in the rib structure. These reinforcements cause surface errors locally around the fittings. Note that although the surface has high frequency content, no consistent quilting appears across the surface.

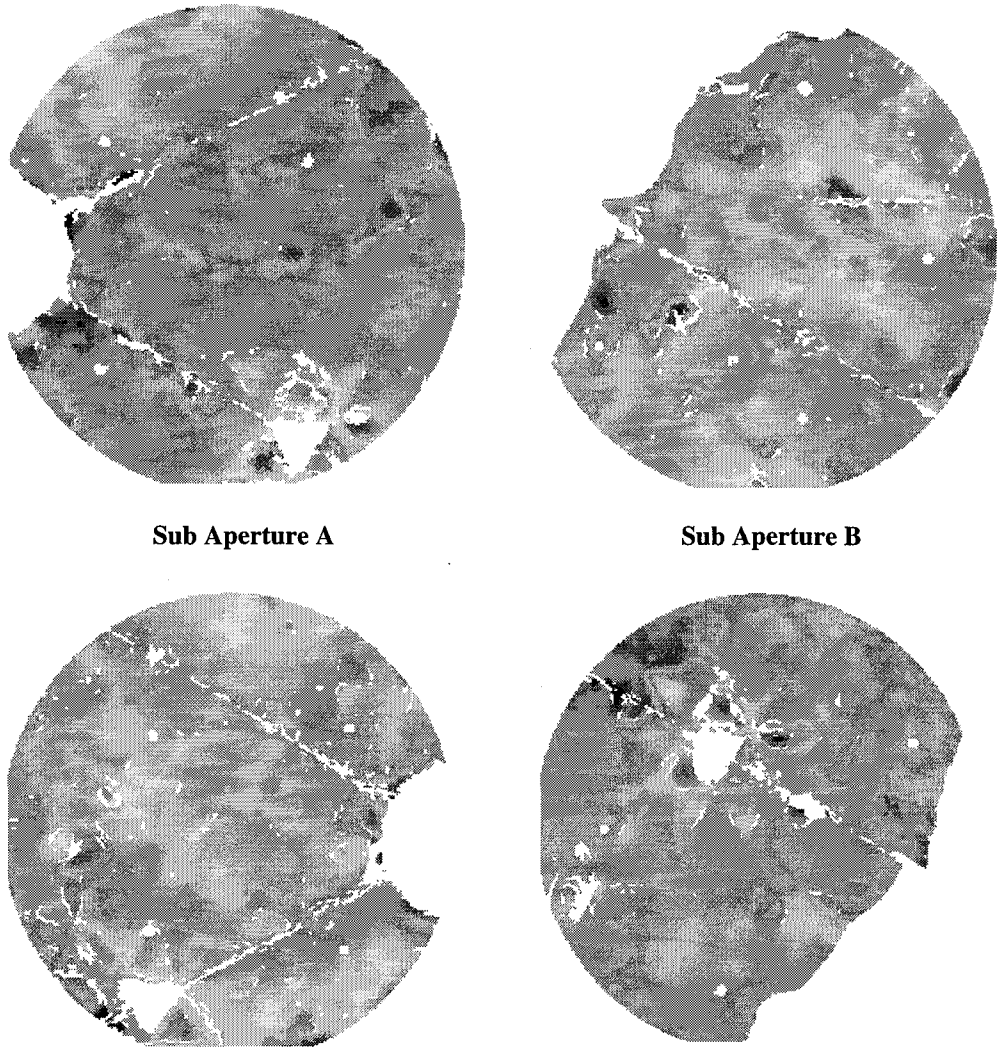

Sub Aperture A **Sub Aperture B**

Sub Aperture C **Sub Aperture D**

Figure 16: Sample of Sub Aperture Surface Data

10. INTERPRETATION OF DATA

The data was interpreted in a four ways:

1. Simulated interferogram at $\lambda = 80\ \mu m$,
2. RMS surface error vs. temperature,
3. PSD at temperature,
4. Cumulative RMS at temperature.

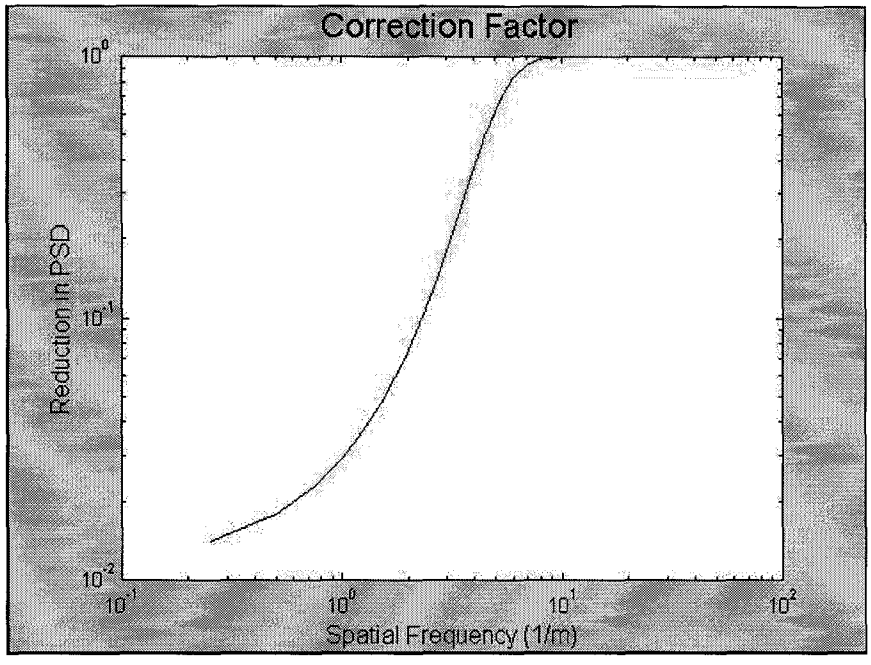

Figure 17: Correction Factor for Telescope with Matched Secondary and Primary Mirrors

When reviewing the surface errors, it is important to also consider the effect of correcting aberrations with the secondary mirror. These corrections are limited by the field of view of the telescope not by the fabrication techniques available for the secondary mirror. A correction factor that represents the improvement in the performance due to a matched secondary can be applied to the RMS, PSD and cumulative RMS. The correction factor is shown in Figure 17.

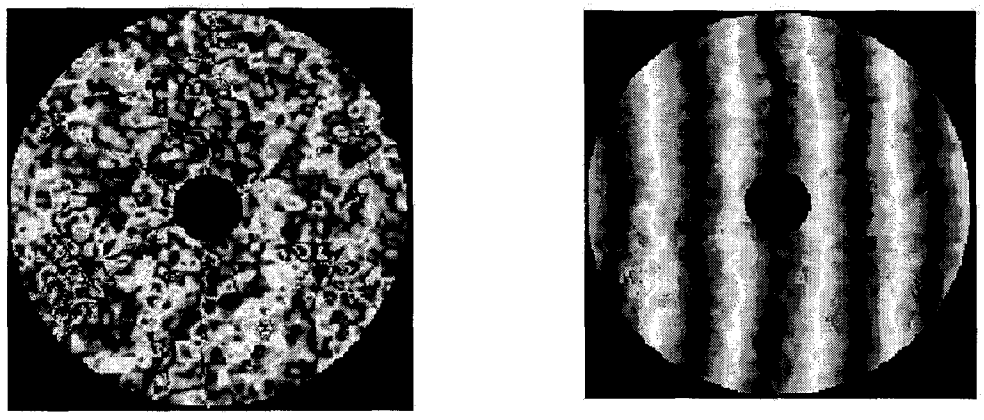

Figure 18: Simulated Interferogram

The interferograms collected using λ = 10.6 μm make a direct interpretation of the performance of the telescope difficult. Since most systems are tested at the wavelength of operation, calculating a simulated interferogram for the surface at λ = 80 μm is instructive. Figure 18 shows this simulated interferogram for the delta surface map from room temperature to 70 K. This interferogram more clearly depicts the mirror as a diffraction limited optic at λ = 80 μm.

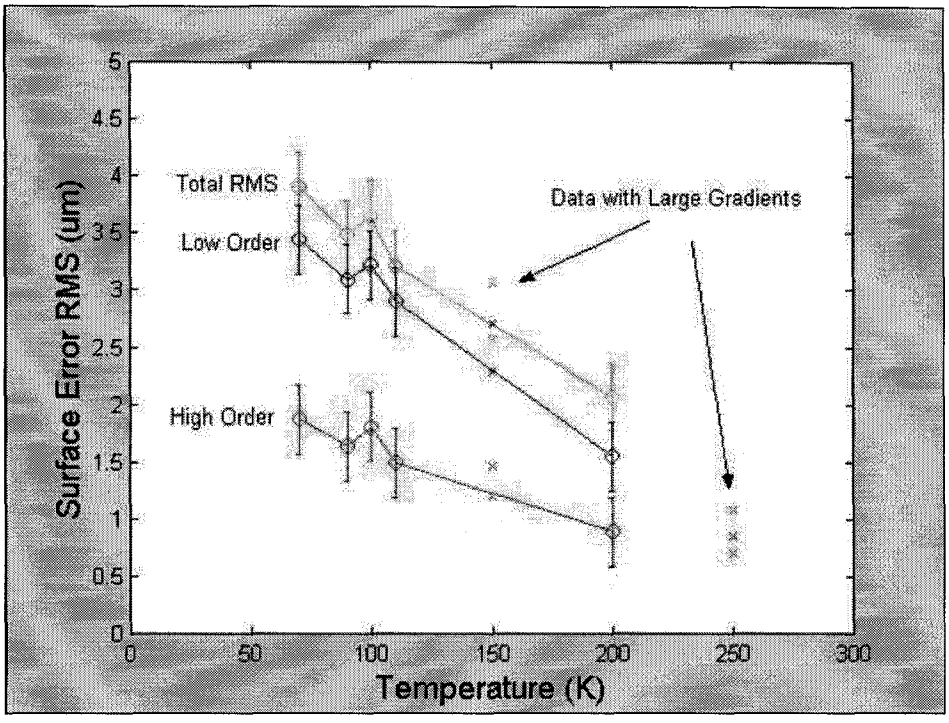

Figure 19: RMS vs. Temperature. Data with Large Thermal Gradients are Shown with an "x"

A plot of the RMS figure error versus temperature helps to understand the trend in surface deformation. Figure 19 illustrates this trend for the first half of the test (room temperature to 70 K). The figure errors are separated into surface error, low order error, and high order error as defined previously. The error bars are based on the random errors characterized previously. Within these error bars, there is a clear linear trend. Some measurements were taken without allowing the temperature to stabilize. These are the points labeled with large thermal gradients. Even these points do not stray far from the linear behavior.

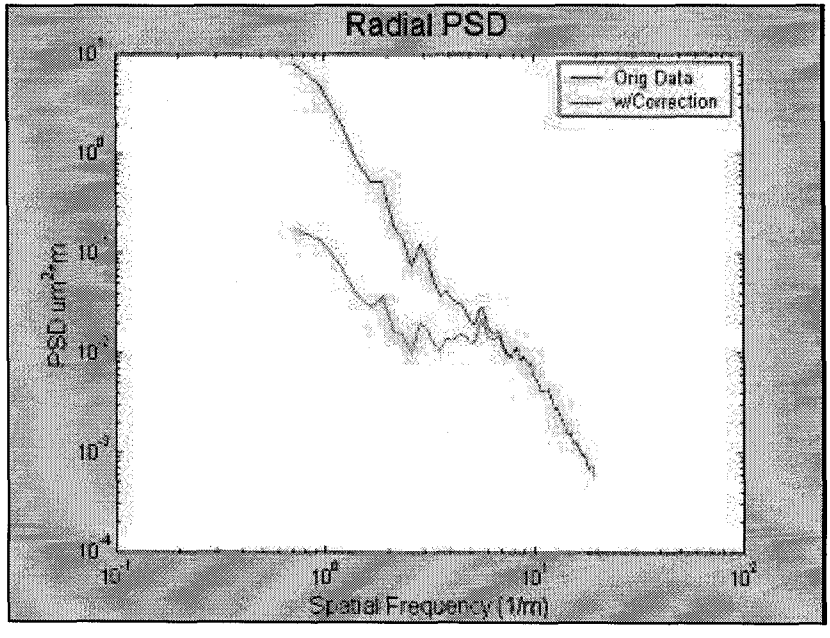

Figure 20: Power Spectral Density (PSD)

The power spectral density (PSD) function is a common method of reviewing the spatial frequency content of an aberrated wavefront. It is essentially the magnitude of the Fourier transform of the surface error. The spatial frequency is traditionally plotted as a function of the radial spatial frequency. The PSD is normalized so that the square root of the integral of the PSD integrated over spatial frequencies is the RMS of the surface. Figure 20 shows both the corrected and uncorrected PSD's. The corrected PSD has a correction factor for a secondary mirror figured to remove low order aberrations from the primary mirror. Note that there are relatively few spikes in the PSD indicating that there is little periodic structure (quilting) to the errors.

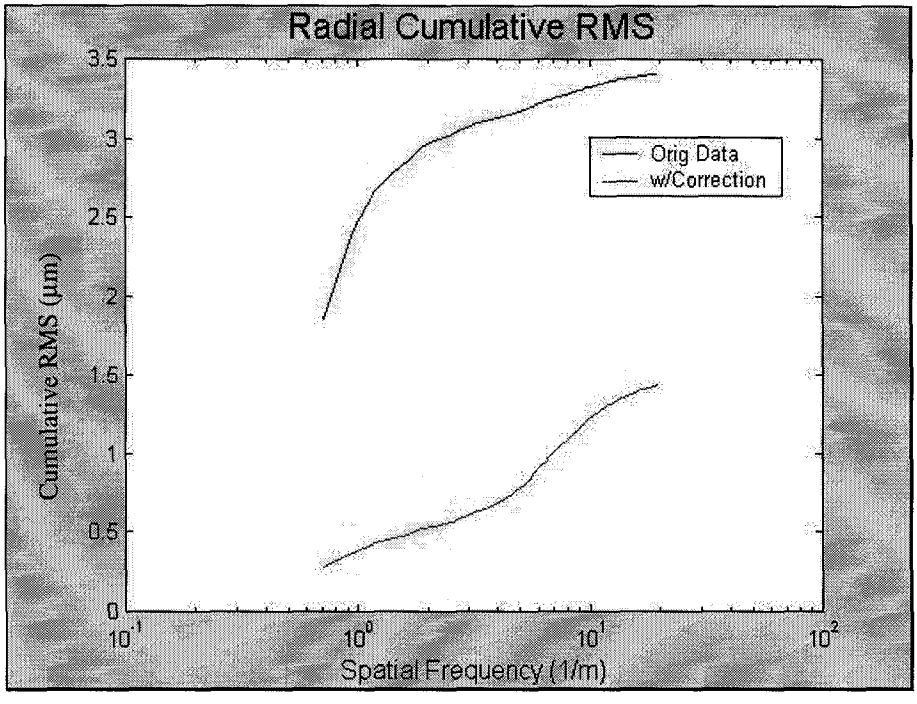

Figure 21: Cumulative RMS vs. Spatial Frequency

In some instances, it is useful to consider the contributions of spatial frequencies (ν) to the RMS. This can be expressed in terms of a Cumulative RMS. The Cumulative RMS is defined as the square root of the integral of the PSD.

$$Cumulative_{RMS}(\nu) = \sqrt{\int_{o}^{\nu} PSD(\nu)d\nu}$$

At $\nu = \infty$, the Cumulative RMS is merely the RMS of the surface. At an intermediate spatial frequency, ν, it is the RMS of the surface including only the contributions from spatial frequencies less than ν. With this type of representation, the contributions of low order and high order frequencies can be more easily visualized. Figure 21 shows the Cumulative RMS for the surface deformation from room temperature to 70 K. The Cumulative RMS after correction is also depicted.

11. CONCLUSION

A unique lightweight mirror fabricated by molding and assembling carbon fiber composite was tested at cryogenic (70 K) temperature. The facility at AEDC was used for this optical test and its dynamic environment was characterized to ensure a vibration free environment. Custom thermal management was designed and implemented to achieve the desired temperature in the required time with small thermal gradients. Using an infrared interferometer, full aperture and sub aperture interferograms were recorded. The surfaces were analyzed and interpreted using simulated interferograms, surface RMS, PSD, and Cumulative RMS. After applying the anticipated corrections on the secondary mirror of the telescope, the figure errors met the requirements for the Herschel Space Observatory telescope.

12. ACKNOWLEDGEMENTS

The work described in this paper was carried out by COI, LWO and JPL (California Institute of Technology), under a contract with the National Aeronautics and Space Administration. Eric Hochberg's critique of the instrumentation and experience measuring CFRP reflectors was greatly valued. Numerous individuals at COI contributed to the overall success of the effort: Robert Dicenso, Steve Prigmore, Dan Federico, Robert Buckner, Dan Highland, and Bill Griffith. James Sisco's (AEDC) support as the lead engineer for the Mark 10V chamber was invaluable to the smooth, efficient operation of the test environment. The authors also wish to thank Pat Woida for his hard work in refurbishing both the Wyko and BRO interferometers and his continued consultations on both interferometers and Raymond Castonguay for his contributions and rapid modifications to the Intelliwave software from Engineering Synthesis Design.

13. REFERENCES

1. E. J. Cohen, S. J. Connell, K. J. Dodson, J. L. Abbot, A. Abusafieh, Z. Backovsky, J. Dyer, J. Escobedo-Torres, Z. Friedman, A. Hull, D. Small, P. Thorndyke, and S. Whitmore "Architecture of the FIRST telescope," SPIE Proceedings Vol 4015, March 2000.
2. S. J. Connell, K. J. Dodson, Z. Friedman, B. Catanzaro, S. Whitmore, and E. J. Cohen "Design progression of an all-composite primary mirror for the FIRST Telescope," SPIE Proceedings Vol 4013, March 2000.
3. B. Catanzaro, J. A. Thomas, D. Small, R. Johnston, D. Barber, S. Connell, S.Whitmore, and E. J. Cohen "Optical metrology for testing an all-composite 2-meter diameter mirror," SPIE Proceedings Vol 4444, August 2001.
4. B. Catanzaro, J. A. Thomas , and E. J. Cohen "Comparison of full-aperture interferometry to sub-aperture stitched interferometry for a large diameter fast mirror," SPIE Proceedings Vol 4444, August 2001.
5. B. Catanzaro, J. Thomas, S. Backovsky, D. Barber, D. Small, R. Johnston, and E. J. Cohen "The effects of aberrations (low order and quilting) on the performance of the all-composite design for the Herschel Space Observatory," SPIE Proceedings Vol 4444, August 2001.